Applied Surface Science 463 (2019) 331–338

Contents lists available at ScienceDirect

Applied Surface Science

journal homepage: www.elsevier.com/locate/apsusc

Full Length Article

Adsorption of lithium polysulfides on an anatase (1 0 1) and an α-Al_2O_3 (0 0 0 1) surface under external electric field with first principles calculations

Dengxin Yan[a,b], Qin Liu[c], Cheng Zeng[d], Ningbo Dong[b], Yudai Huang[a,*], Wei Xiao[c,*]

[a] Key Laboratory of Energy Materials Chemistry, Ministry of Education; Key Laboratory of Advanced Functional Materials, Autonomous Region; Institute of Applied Chemistry, Xinjiang University, Urumqi, 830046 Xinjiang, PR China
[b] Division of Solar Cell, State Power Investment Corporation Research Institute, Beijing 100029, PR China
[c] Division of Nuclear Materials and Fuel, State Power Investment Corporation Research Institute, Beijing 100029, PR China
[d] School of Engineering, Brown University, 184 Hope Street, Providence, RI 02912, United States

ARTICLE INFO

Keywords:
Li–S batteries
Electric field
Adsorption energy
Anatase
α-Al_2O_3
First-principle calculations

ABSTRACT

The "shuttle effect" induced by the dissolution and diffusion of the Li_2S_x ($4 \leqslant x \leqslant 8$) into the electrolyte is a crucial problem of a Li–S battery. Anatase or Al_2O_3 can be used as an additive to suppress the "shuttle effect". First-principles approach coupled with van der Waals (vdW) interaction is used to calculate the adsorption energies of Li_2S_x ($x = 4, 6, 8$) molecules on an anatase (1 0 1) or an α-Al_2O_3 (0 0 0 1) surface. The results show that the adsorption of the molecules on an α-Al_2O_3 (0 0 0 1) is stronger than that on an anatase (1 0 1) surface. Furthermore, owing to the existence of an electric field inside the battery during the charge-discharge process, the external electric field effects on the adsorption are investigated. As a result, the adsorption energy (absolute value) almost linearly increases with the increase of electric field intensity in the range from −0. 16 to 0.16 V/Å. In addition, the responses of different Li_2S_x molecules on an anatase (1 0 1) surface or an α-Al_2O_3 (0 0 0 1) surface to the external electric fields are different.

1. Introduction

Li–S battery is regarded as a promising high-power device in extensive applications, from small mobile devices to large-scale grid energy storage [1,2]. Compared with lithium-ion batteries (LIBs), Li–S batteries exhibit advantages of high theoretical energy density of 2600 W h kg^{-1} (five to seven times higher than that of LIBs) [3–5]. In addition, due to the natural abundance, eco-friendliness, and low cost, sulfur is considered as an ideal cathode material in Li–S batteries [6,7]. All these features make Li–S battery becomes one of the most attractive candidates for next-generation energy storage devices [8].

Despite these advantages of Li–S batteries, difficulties still exist on the practical application. The major challenge for the commercial application of Li–S battery is the dramatic capacity decay [9]. During a Li–S battery discharging process, elemental S is initially reduced to form soluble long chain Li_2S_x ($4 \leqslant X \leqslant 8$) species. These Li_2S_x molecules dissolve into the electrolyte and migrate through the separator, which results "shuttle effect" [10]. In addition, the insulating nature of sulfur (conductivity ~10^{-30} S cm^{-1}) and a large volume expansion by up to ~ 80% upon full lithiation are serious concerns in the sulfur electrode design [11].

Recently, extensive efforts have been devoted to addressing the shortcomings, including preparation of novel composite electrodes [12,13], decoration the separators [14], and anode protection [15,16]. Due to the long-chain lithium polysulfides are highly polar, therefore polar materials (metal oxides) or polar groups should be used to inhibit the shuttling of lithium polysulfides [17]. Some metal oxides with polar surfaces, including $Mg_{0.6}Ni_{0.4}O$, Al_2O_3, MnO_2, V_2O_5, TiS_2, TiO_2 and Co_9S_8 [18–24] have been used as additives or absorbents to inhibit the "shuttle effect". For example, TiO_2 and Al_2O_3 are promising additives due to their strong interaction with lithium polysulfides. Furthermore, TiO_2 is one of important environmental purification photocatalysts because its excellent air pollution control and its ability to fully disintegrate harmful pollutants [25–29]. Gao et al. [30] reported hierarchical TiO_2 sphere-sulfur frameworks assisted with graphene as a cathode material can trap the polysulfides via chemisorption. The interactions between Li_2S_x species and TiO_2 have been studied with experimental and theoretical methods and the results show that TiO_2 and Li_2S_x species can form strong chemical bonds [31]. Yushin et al. [32] reported that Al_2O_3 coated electrodes can improve the cycling

* Corresponding authors.
E-mail addresses: huangyd@xju.edu.cn (Y. Huang), xiaowei1@gmail.com, xiaowei@snptc.com.cn (W. Xiao).

https://doi.org/10.1016/j.apsusc.2018.08.184
Received 30 January 2018; Received in revised form 18 July 2018; Accepted 21 August 2018
Available online 23 August 2018
0169-4332/

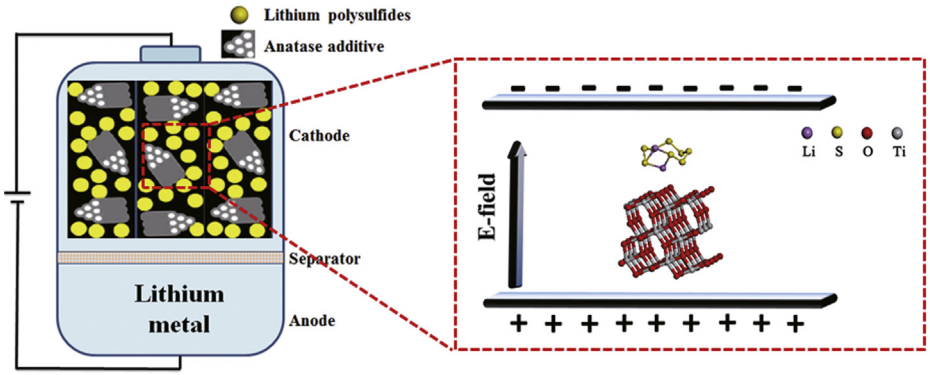

Fig. 1. Schematic illustration a Li_2S_8 molecule is adsorbed on an anatase (1 0 1) surface. The electric field is perpendicular to the anatase (1 0 1) surface.

performance of Li—S batteries, owing to the inhibited deposition of Li_2S on electrodes by Al_2O_3 coating. Chen et al. [33] reported a free-standing Al_2O_3—Li_2S-graphene oxide sponge (GS) composite cathode, in which ultrathin Al_2O_3 films are preferentially coated on Li_2S by an atomic layer deposition (ALD) technique. The results show that the ultra-thin Al_2O_3 film not only acts as a physical barrier to Li_2S nanoparticles, but also provides a strong binding interaction to suppress lithium polysulfides dissolution.

Therefore, it is meaningful to investigate the adsorption between TiO_2/Al_2O_3 and lithium polysulfides. Furthermore, owing to the existence of electric field inside the battery during the process of charging and discharging, it is crucial to investigate the electrical field effects on the adsorption [34,35].

In this paper, first-principles approach coupled with vdW interaction is used to investigate the adsorption of Li_2S_x (x = 4, 6, 8) molecules on an anatase (1 0 1) and an α-Al_2O_3 (0 0 0 1) surface. The results show that the adsorption of the molecules on the α-Al_2O_3 (0 0 0 1) is stronger than that on the anatase (1 0 1) surface. In addition, the external electric field effects on the adsorption of Li_2S_x (x = 4, 6, 8) on an anatase (1 0 1) and an α-Al_2O_3 (0 0 0 1) surface are studied using density functional theory (DFT) calculations. The responses of different Li_2S_x molecules on an anatase (1 0 1) surface or an α-Al_2O_3 (0 0 0 1) surface to the external electric fields are different.

2. Computational details and models

2.1. Calculation details

The adsorption energies of Li_2S_x (x = 4, 6, 8) on an anatase (1 0 1) surface and an α-Al_2O_3 (0 0 0 1) surface are studied with DFT [36,37] calculations, which are performed using Vienna ab initio simulation package (VASP) code [38]. The exchange correlation functional within the generalized gradient approximation (GGA) parameterized by Perdew, Burke, and Enzerof (PBE) [39] is applied in the calculations. The projected augmented wave (PAW) method [40] is used to deal with the wave functions near the core region. The smooth part of the wave function is expanded in plane waves with a kinetic energy cutoff of 400 eV. In order to avoid the periodic interactions between neighbor anatase/α-Al_2O_3 slabs, a vacuum layer with the thickness of 20 Å is on the top the slabs. A grid of 2 × 2 × 1 k-point mesh is used for adsorption calculations. The energy convergence criterion of the self-consistent functional (scf) calculation is 10^{-4} eV. The conjugate gradient method is used to relax the Hellmann-Feynman force in the ionic relaxation with the force stopping criterion of values of 0.05 eV/Å. In order to evaluate the long range effects, some adsorption energies are calculated using the DFT-D3 method with Becke Jonson damping [41], in which the vdW interaction is considered.

DFT calculations underestimate the band gaps of semi-conductor materials. To overcome this problem, on-site Coulomb interactions (DFT + U) [42] are used in the calculations. The U value of 4 eV is applied for the 3d orbital electrons, which enlarges the band gap from 1.1 eV to 2.0 eV. Although we can get gap value which is close to the experimental data with a larger U value, the lattice constants of anatase are not reasonable with this U value [43].

The adsorption energy of a Li_2S_x (x = 4, 6, 8) molecule on an anatase (1 0 1) or an α-Al_2O_3 (0 0 0 1) surface ΔE_{ad} is defined as:

$$\Delta E_{ad} = E_{surf+Li_2S_x} - E_{surf} - E_{Li_2S_x} \quad (1)$$

here $E_{surf+Li_2S_x}$ and E_{surf} are the total energies of an anatase or an α-Al_2O_3 slab with or without adsorbed Li_2S_x molecules, respectively. $E_{Li_2S_x}$ is the energy of an isolated molecule. For the structural optimization of the molecules, the molecules are inside a cubic box of 10 × 10 × 10 $Å^3$.

Because of the physical vdW interaction, the Li_2S_8 and Li_2S_6 molecules deform seriously after adsorbed on two dimensional layered materials [44]. It is suggested that the lying-in-plane Li_2S_x is energetic favorable on surfaces. In addition, Li ions prefer to stay on the O sites and S ions prefer to stay on the Ti or Al sites to form strong chemical bonds. Therefore, Li_2S_x (x = 4, 6, 8) molecules with lying-in-plane configurations on an anatase (1 0 1) or an α-Al_2O_3 (0 0 0 1) surface are used to calculate the adsorption energies. Totally, more than ten initial adsorption configurations of each molecular on an anatase (1 0 1) or an α-Al_2O_3 (0 0 0 1) surface are chosen and then the systems are relaxed (see Tables S1 and S2 in Supporting Information for detail). The system with the lowest system energy is used to study the electric field effects on the adsorption.

The adsorption behaviors are investigated under an external electric field, which is applied in the direction perpendicular to the anatase (1 0 1) surface or the α-Al_2O_3 (0 0 0 1). The schematic of a Li_2S_8 molecule adsorbed on an anatase (1 0 1) surface is shown in Fig. 1. The electric field is perpendicular to the anatase (1 0 1) surface. In our calculations, the adsorption energies are calculated under the electric field intensity of the range from −0. 16 to 0.16 V/Å with a increment of 0.04 V/Å. In addition, external electric field effects on the system energy of the Li_2S_x (x = 4, 6, 8) molecules are evaluated with Gaussian package [45]. The results show that the electric field has little effect on the system energies of the Li_2S_x (x = 4, 6, 8) molecules. As a result, when we calculate the external electric field effects on the adsorption energies of the Li_2S_x (x = 4, 6, 8) molecules on an anatase (1 0 1) or an α-Al_2O_3 (0 0 0 1) surface, the ground state energies of the molecules are used.

In order to evaluate vdW interactions, the vdW interactions effect ratio is defined as:

$$R = \frac{E_{ad}^{vdW} - E_{ad}^{no-vdW}}{E_{ad}^{vdW}} \quad (2)$$

where E_{ad}^{vdW} and E_{ad}^{no-vdW} represent the adsorption energies calculated with and without vdW functional, respectively.

The adsorption energies are calculated with two optimization sequences. For the first relaxation method (Step1), the adsorption energies are directly calculated with or without considering vdW interaction. In the second method (Step2), the adsorption systems are relaxed considering vdW and then final configurations are relaxed again without considering the vdW interaction. When investigating the vdW effects on the adsorption with Eq. (2), E_{ad}^{no-vdW} is obtained from the calculation strategy Step2 and E_{ad}^{vdW} is obtained from calculation strategy Step1.

In the electric field effects calculations the optimized structures (Step1 with vdW) are used, which include the molecules and adsorption systems. These structures are also used in the electronic structure analysis, including charge density difference analysis, PDOS calculation and the Bader charge analysis.

2.2. Calculation models

2.2.1. Structures of an anatase (1 0 1) and an α-Al_2O_3 (0 0 0 1) surface

A 18 atomic layers super cell in which there are six stoichiometric TiO_2 structure layers ($Ti_{36}O_{72}$, 108 atoms) is used to calculate the surface energy and adsorption energies. During the relaxation process, the bottom 6 atomic layers are fixed and the other 12 atomic layers are free to relax. The surface energy of the anatase slab is 0.50 J/m^2, which is close to Lazzeri et al.'s work [46]. Our optimized bulk lattice constants of anatase are a = 3.83 Å, c = 9.62 Å, which are close to the experiment values of a = 3.78 Å, c = 9.51 Å [47].

A 9 atomic layers α-Al_2O_3 (0 0 0 1) ($Al_{54}O_{81}$, 135 atoms) model is used to calculate the surface energy and the adsorption energies. The surface energy of the α-Al_2O_3 slab is 1.47 J/m^2, which is close to Siegel et al.'s computational result of 1.50 J/m^2 [48]. The optimized bulk lattice constants of α-Al_2O_3 in this work are a = 4.765 Å, c = 12.998 Å, which are close to the experiment values of a = 4.758 Å, c = 13.00 Å [49].

2.2.2. Structures of S_8 and Li_2S_x ($1 \leqslant x \leq 8$) molecules

The S_8 and Li_2S_x ($1 \leqslant x \leq 8$) represent the critical lithiation stages in Li–S battery [50], which have been studied with computational methods [51,52]. The geometric structures of S_8 and Li_2S_x ($1 \leqslant x \leq 8$) are optimized and the configurations after relaxation are listed in Fig. 2.

The most stable structure of S_8 is the D_{4d} symmetry, and the S–S bond length and S–S–S bond angle are 2.06 Å and 109.6°, respectively. The most stable structures of Li_2S and Li_2S_2 are the C_{2V} symmetry. The most stable structures of Li_2S_x (x = 4, 6, 8) are the C_2 symmetry.

The shortest Li–S bond length in each molecule are 2.12 Å for Li_2S, 2.24 Å for Li_2S_2, and 2.36 (2.42 and 2.37) Å for Li_2S_4 (Li_2S_6 and Li_2S_8) and the bond angle of Li–S–Li are 108° for Li_2S, 98.5° for Li_2S_2, and 73.8° (68.8° and 66.3°) for Li_2S_4 (Li_2S_6 and Li_2S_8). These results agree with Assary and Wang et al.'s theoretical results [53,54].

In the discharging of Li–S batteries, S–S covalent bonds of Cycloocta-S molecule are broken and Li_2S_x ($2 \leqslant x \leq 8$) molecules formed, which are reduced to Li_2S eventually. The Li–S bonds length of the long-chain Li_2S_x (x = 4, 6, 8) molecules are longer than the short-chain molecules (Li_2S and Li_2S_2), which implied a weaker interaction between Li and S for long-chain compounds. Compared with Li_2S or Li_2S_2, the long-chain Li_2S_x (x = 4, 6, 8) clusters are more easily ionized into Li and polysulfide ions in an electrolyte solution, leading to the so-called "shuttle effect" during the redox process.

2.2.3. Structures of Li_2S_x (x = 4, 6, 8) molecules on an anatase (1 0 1) or an α-Al_2O_3 (0 0 0 1) surface

Fig. 3(a) exhibits the top and side views of the Li_2S_x (x = 4, 6, 8) species on anatase (1 0 1) supercell before structural optimization. Fig. 3(b) exhibits the top and side views of the Li_2S_x (x = 4, 6, 8) species on α-Al_2O_3 (0 0 0 1) supercell before structural optimization.

3. Results and discussion

3.1. Adsorption of Li_2S_x (x = 4, 6, 8) molecules on an anatase (1 0 1) or an α-Al_2O_3 (0 0 0 1) surface

The adsorption energies of Li_2S_x (x = 4, 6, 8) molecules on an anatase (1 0 1) surface and an α-Al_2O_3 (0 0 0 1) surface are investigated in this section. The adsorption energies of these molecules on the two slabs are calculated and plotted in Fig. 4 and the data are listed in Table 1. In Fig. 4, the adsorption of the molecules on the α-Al_2O_3 (0 0 0 1) is stronger than that on the anatase (1 0 1) surface. For the three molecules, Li_2S_6 is the most strongly adsorbed on the surfaces compared with the other two molecules. The chemical bonding of the Li_2S_6/Li_2S_8 on the α-Al_2O_3 (0 0 0 1) surface exceed 4 eV in the ground state. If the chemical bonding energy is higher than 2 eV, a Li_2S_x molecule is strongly adsorbed on the surface of matrix material and Li–S bond is weakened, which induces the separation between lithium and sulfur atoms and sulfur material can dissolve into the electrolyte [44]. Once the Li_2S_x species decompose and Li^+ and S_x^{2-} ions form, the capacity of the battery decays [31,44].

Consider the vdW interaction in the adsorption process, the adsorption energies are re-calculated and plotted as the dash lines in Fig. 4. It shows that the adsorption energies are more negative or the adsorption processes are stronger if vdW is considered in the calculations. Our calculated adsorption energies are listed in Table 1. The vdW interaction effect is very strong for Li_2S_8, which is the biggest molecule in our calculations. As Zhang et al., claim that the chemical interaction mainly comes from the lithium ions and the physical interaction is largely contributed by sulfur atoms [44]. With most number of sulfur atoms, the adsorption energy of Li_2S_8 on an anatase (1 0 1) surface is mainly from sulfur atoms. The second observation is that the vdW interaction effect on an anatase (1 0 1) surface is stronger than that on an α-Al_2O_3 (0 0 0 1) surface, especially for the Li_2S_8 molecule.

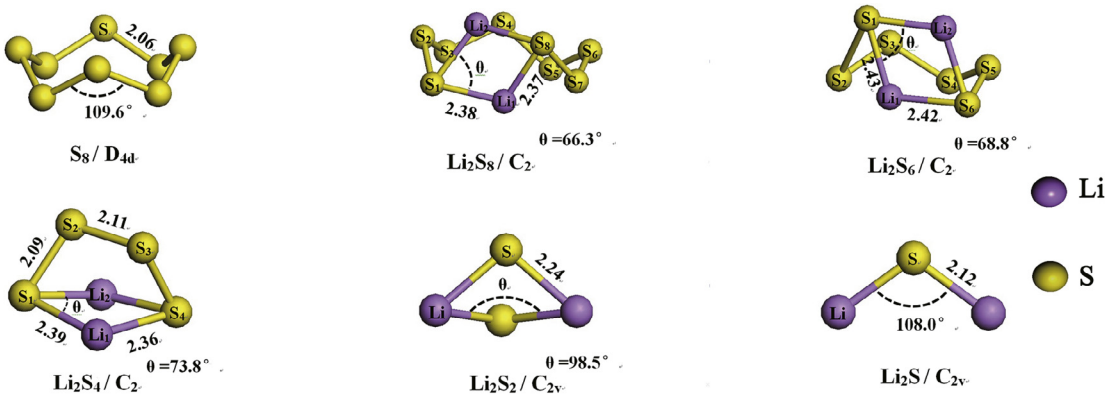

Fig. 2. Optimized configurations of Li_2S_x ($1 \leqslant x \leqslant 8$) molecules. The symmetry groups, bond lengths, and bond angles are shown.

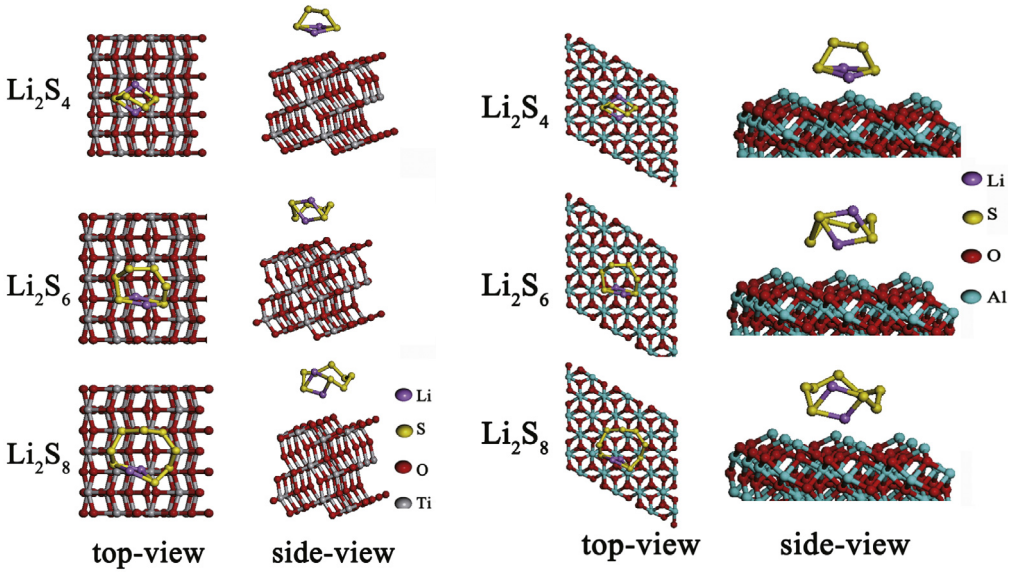

(a) Li_2S_x on an anatase (101) surface (b) Li_2S_x on an α-Al_2O_3 (0001) surface

Fig. 3. Top and side views of (a) anatase (1 0 1) and (b) α-Al_2O_3 (0 0 0 1) supercell with Li_2S_x (x = 4, 6, 8) species before structural optimization.

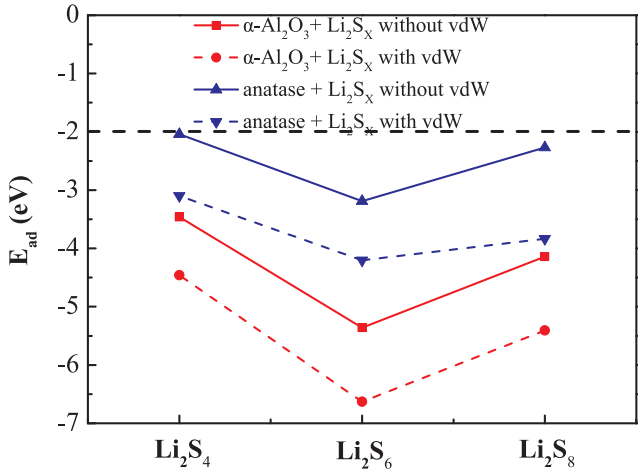

Fig. 4. Adsorption energies of the molecules Li_2S_x (x = 4, 6, 8) on an anatase (1 0 1) surface and an α-Al_2O_3 (0 0 0 1) surface. The effect of vdW interaction on the adsorption energy is evaluated.

The configurations of Li_2S_x (x = 4, 6, 8) on an anatase (1 0 1) surface and an α-Al_2O_3 (0 0 0 1) surface optimized with and without vdW functional are shown in Fig. 5. As the biggest molecule, the Li_2S_8 seriously deforms on the anatase (1 0 1) surface and the physical vdW interaction plays an important major role in this process (Fig. 5(a)). For a Li_2S_4 on an anatase (1 0 1) surface, the adsorption configuration relaxed considering vdW is almost the same as that without vdW interaction calculations involved because chemical interaction dominates (Fig. 5(a)). On the contrary, the vdW interaction effect is not important for Li_2S_x (x = 4, 6, 8) adsorption on the α-Al_2O_3 (0 0 0 1) surface because chemical interaction dominates (Fig. 5(b)).

To clearly investigate the formation of chemical bonds between the Li_2S_x (x = 4, 6, 8) molecules and surface, the partial density of states (PDOS) of the Li, S, Ti, Al and O atoms were determined and are depicted in Figs. 6 and 7.

In Fig. 6, panels (a–c) represent the PDOS plots for relaxed structures of Li_2S_4, Li_2S_6 and Li_2S_8 absorbed on anatase (1 0 1) surface. For the Li_2S_8 on an anatase (1 0 1) surface, PDOS calculation shows that there are peaks near the Fermi energy for both S atom and the Ti atom (see Fig. 6(c)). Also, two small peaks for a Li atom and an oxygen atom are also close to the Fermi energy. The bond length of S—Ti bond is 2.50 Å and that of S—O bond is 3.02 Å. The bond length of Li—O bond is 1.97 Å. So, it suggests that a S—Ti and a Li—O bond form on the surface.

In Fig. 7, panels (a–c) represent the PDOS plots for relaxed structures of Li_2S_4, Li_2S_6 and Li_2S_8 absorbed on the α-Al_2O_3 (0 0 0 1) surface. For the Li_2S_8 on an α-Al_2O_3 (0 0 0 1) surface, PDOS calculation shows that there are peaks near the Fermi energy for both the S atom and the Al atom (see Fig. 7(c)). Also, two small peaks for a Li atom and an oxygen atom are also close to the Fermi energy. The bond length of S—Al bond is 2.25 Å and that of S—O bond is 3.25 Å. The bond length of Li—O bond is 2.3 Å. So, it suggests that a S—Al and a Li—O bond form on the surface.

To quantify the redistribution of electron density delocalization upon the adsorption of molecules on surface, the Bader charge analysis has been performed for the optimized adsorption configurations. The

Table 1
Adsorption energies (eV) of the Li_2S_x (x = 4, 6, 8) molecules on an anatase (1 0 1) (E_{ad101}) and an α-Al_2O_3 (0 0 0 1) (E_{ad0001}) surface. Step1a represents the adsorption energies calculated only one step which without considering the vdW interaction, while Step1b represents the similar calculations considering vdW interaction. The vdW interaction effect ratios R from Eq. (2) are calculated and listed.

Molecules	E_{ad101} (eV)				E_{ad0001} (eV)			
	Step1a	Step1b	Step2	R	Step1a	Step1b	Step2	R
Li_2S_4	−2.02	−3.10	−2.04	34.19%	−3.44	−4.46	−3.46	22.42%
Li_2S_6	−3.16	−4.20	−3.19	24.05%	−5.13	−6.63	−5.36	19.16%
Li_2S_8	−1.25	−3.84	−2.27	40.89%	−4.04	−5.41	−4.14	23.48%

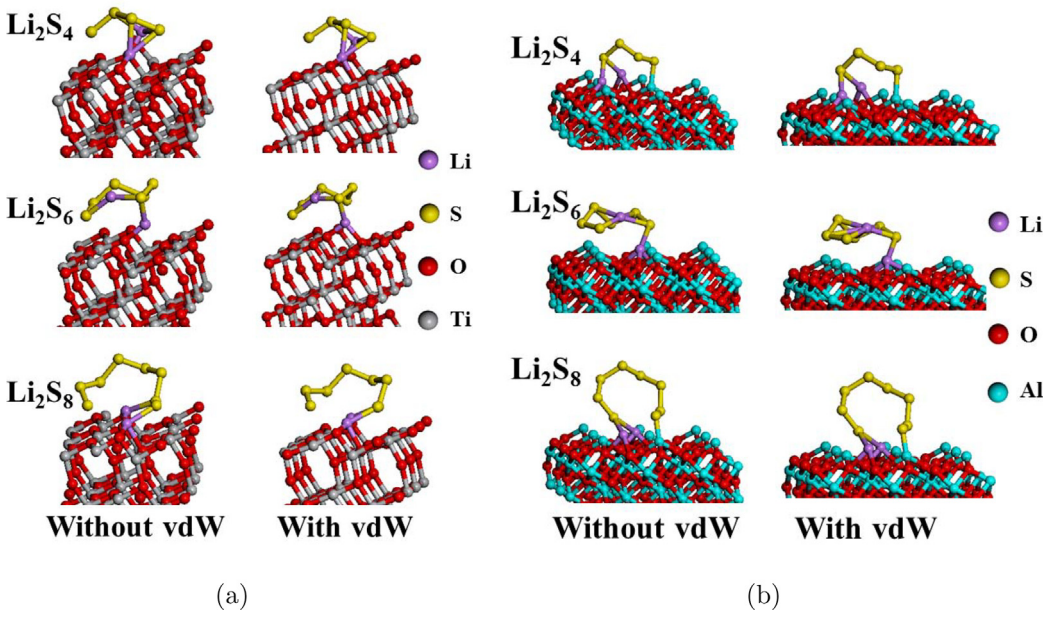

Fig. 5. Li_2S_x (x = 4, 6, 8) molecules adsorbed on (a) an anatase (1 0 1) surface and (b) an α-Al_2O_3 (0 0 0 1) surface after relaxation with (Step1) or without (Step2) considering vdW interaction.

results indicate that the charges transfer from the molecules to the slab and chemical adsorption happens. The charge density difference maps for the adsorption configurations are provided as supplemental documents in Figs. S1 and S2. The results show that the charge is transferred from the molecules Li_2S_x (x = 4, 6, 8) to the anatase (1 0 1) or the α-Al_2O_3 (0 0 0 1) surface. The results are consistent with PDOS

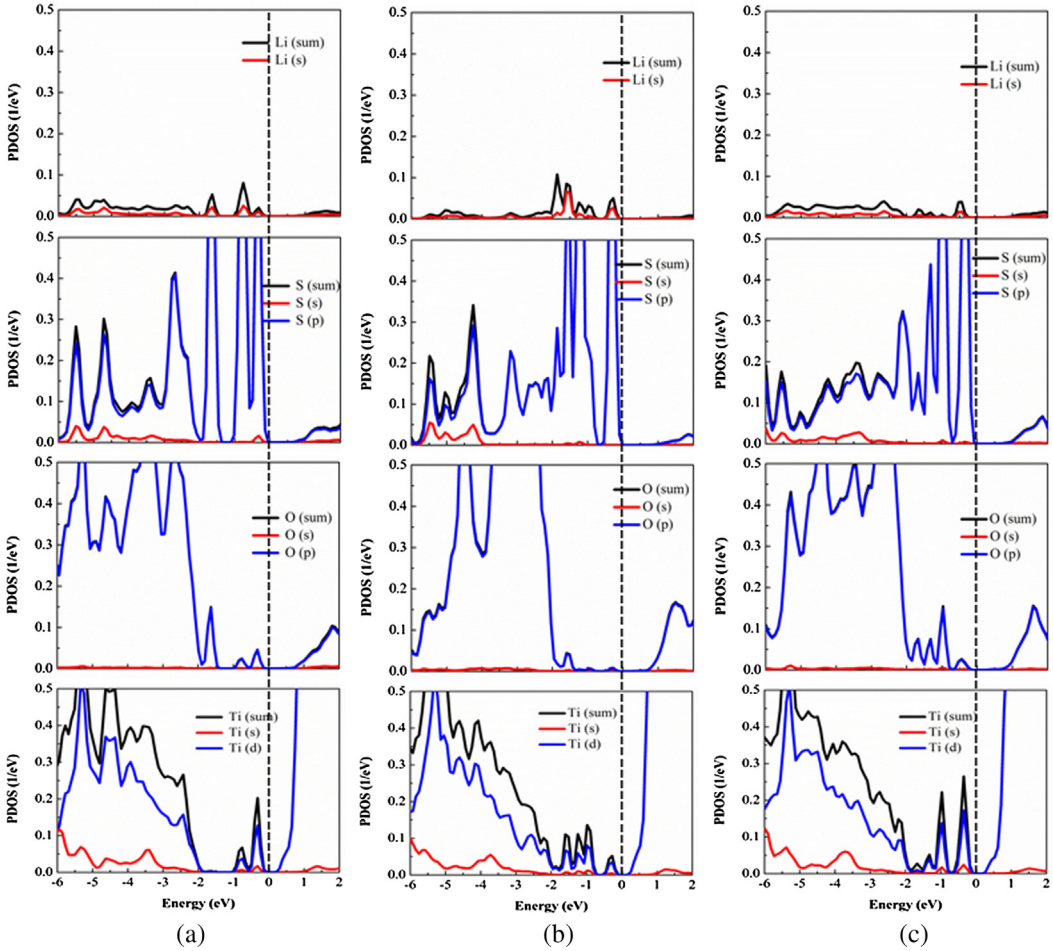

Fig. 6. PDOSs for the adsorption of Li_2S_x (x = 4, 6, 8) on an anatase (1 0 1) surface. (a) Li_2S_4, (b) Li_2S_6, and (c) Li_2S_8.

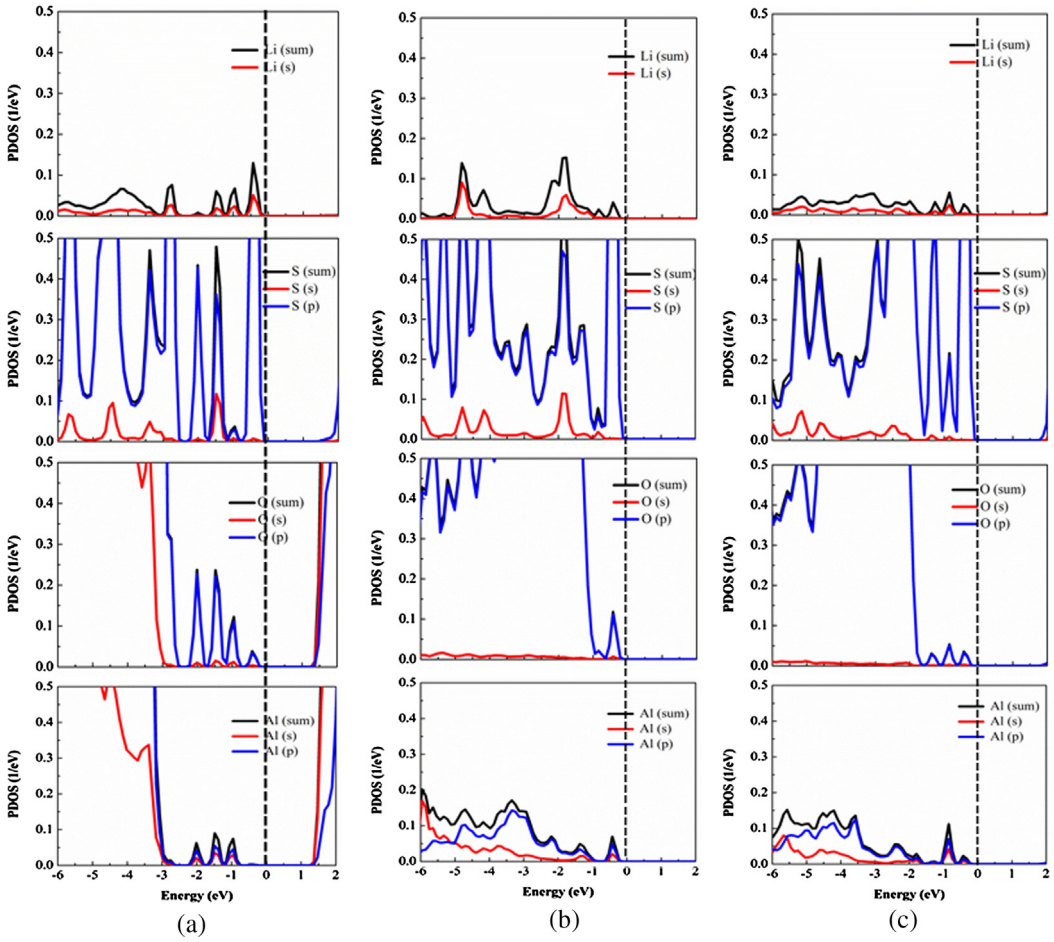

Fig. 7. PDOSs for the adsorption of Li_2S_x (x = 4, 6, 8) on an α-Al_2O_3 (0 0 0 1) surface. (a) Li_2S_4, (b) Li_2S_6, and (c) Li_2S_8.

calculation and the Bader charge analysis.

3.2. Adsorptions in an external electric field

3.2.1. External electric field effects on the adsorption of the Li_2S_x (x = 4, 6, 8) molecules on an anatase (1 0 1) surface

During the running time, the molecules are adsorbed on an anatase surface in an electric field inside the battery. In order to investigate the electric field effects on the adsorption system, the adsorption energies in an electric field are calculated. As mentioned before, the external electric field is perpendicular to the slab (see Fig. 1). The adsorption energies of Li_2S_x (x = 4, 6, 8) on an anatase (1 0 1) surface under external electric field are shown in Fig. 8. The adsorption energy (absolute value) almost linearly increases under the electric field intensity of the range from −0. 16 to 0.16 V/Å. Especially, the adsorption energy of the Li_2S_4 on an anatase (1 0 1) surface is in the range from −0. 75 eV to −5. 47 eV. This large difference suggests that external electric field is important for the adsorption process in a battery.

Our results show that if the direction of the external electric field is from the slab to the molecule, the adsorption energies of the Li_2S_x (x = 4, 6, 8) on an anatase (1 0 1) surface are enhanced. Due to the polarization of the molecule on the surface, the electrons of the molecule may move towards to the slab and the adsorption is enhanced. The other observation is that the slopes of the curves are different in Fig. 8. It suggests that the external electric field responses are different for different molecules. On an anatase (1 0 1) surface, the response for Li_2S_4 is the most serious.

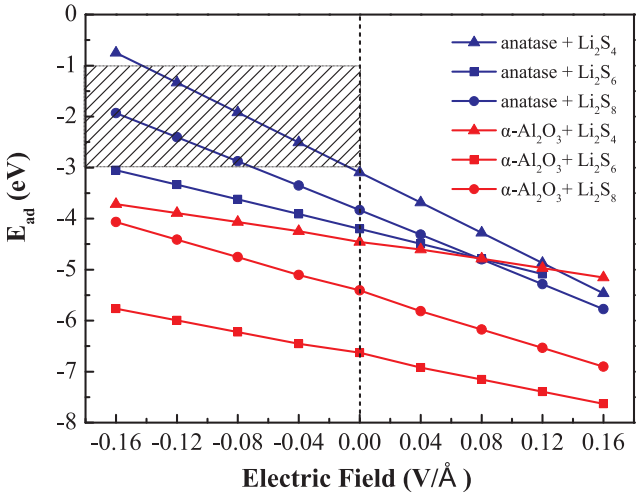

Fig. 8. External electric field effects on the adsorption of the Li_2S_x (x = 4, 6, 8) molecules on an anatase (1 0 1) surface or an α-Al_2O_3 (0 0 0 1) surface.

3.2.2. External electric field effects on the adsorption of the Li_2S_x (x = 4, 6, 8) molecules on an α-Al_2O_3 (0 0 0 1) surface

Similarly, the adsorption energies of Li_2S_x (x = 4, 6, 8) on an α-Al_2O_3 (0 0 0 1) surface almost linearly increase with the change of the electric field from −0. 16 to 0.16 V/Å (see Fig. 8). For example, in this range of external electric filed, the adsorption energy of a Li_2S_8 on an α-Al_2O_3 (0 0 0 1) surface is in the range of −4. 07 eV to −6. 90 eV. The biggest adsorption energy change is about 3 eV in an external electric

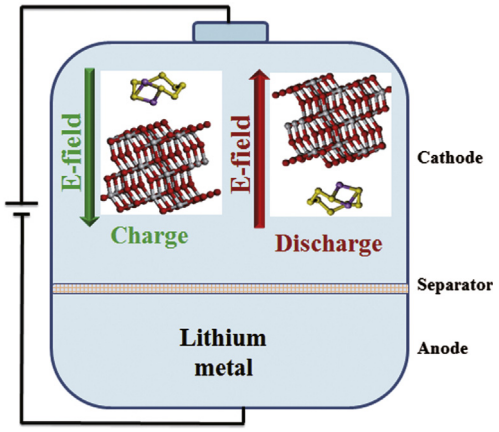

Fig. 9. Schematic diagram of a Li−S battery. When the battery charge/discharge, the direction of the electric field is vertical downward/upward. Parts of the lithium polysulfides in a particular direction are adsorbed with reasonable adsorption energies, which reduces the possibility of shuttling of the lithium polysulfides in charging and discharging process of the Li−S battery.

field. The slopes of the three samples are different. That is, the responses for the external electric field are different for the three molecules on an α-Al_2O_3 (0 0 0 1) surface.

Our simulation results clearly show that the external electric field enhances the adsorption of the Li_2S_x (x = 4, 6, 8) on not only the anatase (1 0 1) but also the α-Al_2O_3 (0 0 0 1) surface. With the external electric field changing from −0. 16 to 0.16 V/Å, the adsorption energies of the Li_2S_x (x = 4, 6, 8) on anatase (1 0 1) or α-Al_2O_3 (0 0 0 1) surface increase almost linearly.

Suppose anatase or Al_2O_3 is used as an absorbent or additive to suppress the diffusion of the Li_2S_x ($4 \leqslant \times \leqslant 8$) in the cathode area of a Li−S batteries. Since the structure of the cathode material is complex, the configurations of the Li_2S_x (x = 4, 6, 8) molecules associated with the additives are also complex. A schematic of Li−S battery is shown in Fig. 9. In this schematic if the battery charging, the direction of the electric field is towards the slab. Under this condition, the external electrical field is negative. As a result, the range of the adsorption energies of the Li_2S_8 and Li_2S_4 on an anatase (1 0 1) surface is in the range of −1 to −3 eV (see Fig. 8). The adsorption energies in this range are good for resolve the shuttle effect of Li−S battery. Similarly, the adsorption energies of the Li_2S_8 and Li_2S_4 on the upper side of an anatase (1 0 1) surface are in the favorable region during discharging (see right side of Fig. 9). Our simulation results suggest that parts of the lithium polysulfides in the particular direction are adsorbed with reasonable adsorption energies, and the possibility of shuttling of the lithium polysulfides are reduced in charging and discharging process of the battery. If the chemical bonding energy is higher than 2 eV, a Li_2S_x molecule is strongly adsorbed on the surface of matrix material and Li−S bond is weakened, which induces the separation between lithium and sulfur atoms and sulfur material can dissolve into the electrolyte [44]. Furthermore, once the Li_2S_x species decompose and Li^+ and S_x^{2-} ions form, the capacity of the battery decays [31,44].

4. Conclusions

In summary, the adsorption energies of Li_2S_x (x = 4, 6, 8) molecules on an anatase (1 0 1) surface or an Al_2O_3 (0 0 0 1) surface under external electrical fields are calculated with first principles calculations. Our results show that the adsorption energies of the Li_2S_x (x = 4, 6, 8) on an α-Al_2O_3 (0 0 0 1) are stronger than that on an anatase (1 0 1) surface. Furthermore, the adsorption energy (absolute value) almost increases linearly with the increase of electrical field intensity from −0. 16 to 0.16 V/Å. The responses of the adsorption of Li_2S_x (x = 4, 6, 8) on an anatase (1 0 1) surface or an α-Al_2O_3 (0 0 0 1) surface to the external electric fields are different.

Acknowledgments

This work is supported by the Essential Research Fund of State Nuclear Power Technology Company, China (SNPTC) under Contract No. C-ZY05-201701. It is also financially supported by the National Natural Science Foundation of China (21466036), the Nature Science Foundation of Xinjiang Province (2015211C286 and 2017D01C074), and the Young Scholar Science Foundation of Xinjiang Educational Institutions (XJEDU2016S030).

Appendix A. Supplementary material

Supplementary data associated with this article can be found, in the online version, at https://doi.org/10.1016/j.apsusc.2018.08.184.

References

[1] P.G. Bruce, S.A. Freunberger, L.J. Hardwick, J.M. Tarascon, Nat. Mater. 11 (1) (2012) 19–29.
[2] Q. Wang, Z.B. Wang, C. Li, D.M. Gu, J. Mater. Chem. A 5 (13) (2017) 6052–6059.
[3] Y. Du, Z. Yin, X. Rui, Z. Zeng, X.J. Wu, J. Liu, Y. Zhu, J. Zhu, X. Huang, Q. Yan, Nanoscale 5 (4) (2013) 1456–1459.
[4] N. Liu, X. Mamat, R. Jiang, W. Tong, Y. Huang, D. Jia, Y. Li, L. Wang, T. Wagberg, G. Hu, Chem. Eng. J. 343 (2018) 78–85.
[5] Y. Cai, Y. Huang, W. Jia, Y. Zhang, X. Wang, Y. Guo, D. Jia, W. Pang, Z. Guo, L. Wang, J. Mater. Chem. A 4 (45) (2016) 17782–17790.
[6] J. Coetzer, Electrochim. Acta 23 (8) (1978) 787–789.
[7] T. Zhao, Y. Ye, X. Peng, G. Divitini, H.-K. Kim, C.-Y. Lao, P.R. Coxon, K. Xi, Y. Liu, C. Ducati, Adv. Funct. Mater. 26 (46) (2016) 8564.
[8] C. Zhang, H.B. Wu, C. Yuan, Z. Guo, X.W. Lou, Angew. Chem. 51 (38) (2012) 9592–9595.
[9] Y. Ye, L. Wang, L.L. Guan, F. Wu, J. Qian, T. Zhao, X. Zhang, Y. Xing, J. Shi, L. Li, Energy Storage Mater. 9 (2017) 126–133.
[10] Q. Wang, M. Yang, Z.B. Wang, C. Li, D.M. Gu, Small 14 (11) (2018) 1703279–1703286.
[11] A. Manthiram, Y. Fu, S.H. Chung, C. Zu, Y.S. Su, Chem. Rev. 114 (23) (2014) 11751–11787.
[12] G. Li, J. Sun, W. Hou, S. Jiang, H. Yong, J. Geng, Nat. Commun. 7 (2016) 10601–10611.
[13] Y. Lu, Y. Huang, Y. Zhang, Y. Cai, X. Wang, Y. Guo, D. Jia, X. Tang, Ceram. Int. 42 (9) (2016) 11482–11485.
[14] J. Li, Y. Huang, S. Zhang, W. Jia, X. Wang, Y. Guo, D. Jia, L. Wang, ACS Appl. Mater. Interfaces 9 (8) (2017) 7499–7504.
[15] S. Xiong, K. Xie, Y. Diao, X. Hong, Electrochim. Acta 83 (12) (2012) 78–86.
[16] W. Li, H. Yao, K. Yan, G. Zheng, Z. Liang, Y.M. Chiang, Y. Cui, Nat. Commun. 6 (2015) 7436–7444.
[17] L. Z, Z. J, L. XW, Angew. Chem. 54 (44) (2015) 12886–12890.
[18] Y. Zhang, Z. Bakenov, Y. Zhao, A. Konarov, T.N.L. Doan, K.E.K. Sun, A. Yermukhambetova, P. Chen, Powder Technol. 235 (2) (2013) 248–255.
[19] M. Yu, W. Yuan, C. Li, J.D. Hong, G. Shi, J. Mater. Chem. A 2 (20) (2014) 7360–7366.
[20] W. Li, J. Hicksgarner, J. Wang, J. Liu, A.F. Gross, E. Sherman, J. Graetz, J.J. Vajo, P. Liu, Chem. Mater. 26 (11) (2014) 3403–3410.
[21] L. Ma, S. Wei, H.L. Zhuang, K.E. Hendrickson, R.G. Hennig, L.A. Archer, J. Mater. Chem. A 3 (39) (2015) 19857–19866.
[22] L. Yong, D. Ye, L. Wen, B. Shi, G. Rui, H. Zhao, H. Pei, J. Xu, Y.X. Jing, ACS Appl. Mater. Interfaces 8 (42) (2016) 28566–28573.
[23] X. He, H. Hou, X. Yuan, L. Huang, J. Hu, B. Liu, J. Xu, J. Xie, J. Yang, S. Liang, Sci. Rep. 7 (2017) 40679–40688.
[24] W. Tong, Y. Huang, W. Jia, X. Wang, Y. Guo, Z. Sun, D. Jia, J. Zong, J. Alloys Compd. 731 (2017) 964–970.
[25] A. Abbasi, J.J. Sardroodi, Sulfur Rep. 38 (1) (2016) 52–68.
[26] A. Abbasi, J.J. Sardroodi, Environ. Sci. Nano 3 (5) (2016) 1153–1164.
[27] A. Abbasi, J.J. Sardroodi, New J. Chem. 41 (21) (2017) 12569–12580.
[28] A. Abbasi, J.J. Sardroodi, Appl. Surf. Sci. 436 (2018) 27–41.
[29] A. Abbasi, J.J. Sardroodi, Comput. Theor. Chem. 1114 (2017) 8–19.
[30] L. Gao, M. Cao, Y.Q. Fu, Z. Zhong, Y. Shen, M. Wang, J. Mater. Chem. A 4 (42) (2016) 16454–16461.
[31] M. Yu, J. Ma, H. Song, A. Wang, F. Tian, Y. Wang, H. Qiu, R. Wang, Energy Environ. Sci. 9 (4) (2016) 1495–1503.
[32] H. Kim, J.T. Lee, D.-C. Lee, A. Magasinski, W.-I. Cho, G. Yushin, Adv. Energy Mater. 3 (10) (2013) 1308–1315.
[33] Y. Chen, S. Lu, J. Zhou, X. Wu, W. Qin, O. Ogoke, G. Wu, J. Mater. Chem. A 5 (1) (2016) 102–112.
[34] W. Shi, Z. Wang, Z. Li, Y.Q. Fu, Mater. Chem. Phys. 183 (2016) 392–397.
[35] W. Shi, Z. Wang, Y.Q. Fu, J. Nanopart. Res. 11 (18) (2016) 1–7.
[36] P. Hohenberg, W. Kohn, Phys. Rev. 136 (3B) (1964) B864–B871.
[37] W. Kohn, L.J. Sham, Phys. Rev. 140 (4A) (1965) A1133–A1138.

[38] G. Kresse, J. Hafner, Phys. Rev.B 47 (1) (1993) 558–561.
[39] J.P. Perdew, K. Burke, M. Ernzerhof, Phys. Rev. Lett. 77 (18) (1996) 3865–3868.
[40] P.E. Blöchl, Phys. Rev. B 50 (24) (1994) 17953–17979.
[41] S. Grimme, J. Antony, S. Ehrlich, H. Krieg, J. Chem. Phys. 132 (15) (2010) 154104–154123.
[42] S. Shi, J. Gao, Y. Liu, Y. Zhao, Q. Wu, W. Ju, C. Ouyang, R. Xiao, Chin. Phys. B 25 (1) (2016) 18212–18236.
[43] Y. Ortega, D.F. Hevia, J. Oviedo, M.A. San-Miguel, Appl. Surf. Sci. 294 (3) (2014) 42–48.
[44] Q. Zhang, Y. Wang, W.S. Zhi, Z. Fu, R. Zhang, Y. Cui, Nano Lett. 15 (6) (2015) 3780–3786.
[45] D. Rao, Y. Wang, L. Zhang, S. Yao, X. Qian, X. Xi, K. Xiao, K. Deng, X. Shen, R. Lu, Carbon 110 (2016) 207–214.
[46] M. Lazzeri, A. Vittadini, A. Selloni, Phys. Rev. B 65 (11) (2001) 155409–155418.
[47] J.K. Burdett, T. Hughbanks, G.J. Miller, J.W.R. Jr, J.V. Smith, Cheminform 18 (37) (1987) 3639–3646.
[48] D.J. Siegel, L.G.H. Jr, J.B. Adams, Phys. Rev. B 654 (8) (2002) 85415–85434.
[49] J.C. Boettger, Phys. Rev. B 55 (2) (1997) 750–756.
[50] C. Barchasz, F. Molton, C. Duboc, J.C. Leprtre, S. Patoux, F. Alloin, A. Chem, Anal. Chem. 84 (9) (2012) 3973–3980.
[51] X. Tao, J. Wang, C. Liu, H. Wang, H. Yao, G. Zheng, Z.W. Seh, Q. Cai, W. Li, G. Zhou, et al., Nat. Commun. 7 (2016) 11203–11211.
[52] T.-Z. Hou, X. Chen, H.-J. Peng, J.-Q. Huang, B.-Q. Li, Q. Zhang, B. Li, Small 12 (24) (2016) 3283–3291.
[53] R.S. Assary, L.A. Curtiss, J.S. Moore, J. Phys. Chem. C 118 (22) (2014) 11545–11558.
[54] B. Wang, S.M. Alhassan, S.T. Pantelides, Phys. Rev. Appl. 2 (3) (2014) 34004–35014.